

## Green Synthesis of Zinc Oxide Nanoparticles Using *Ixora Coccinea* Leaf Extract for Ethanol Vapour Sensing

Leela Pradhan Joshi, Bal Vikram Khatri, Sumana Gyawali, Shiromani Gajurel,  
and Dinesh Kumar Chaudhary\*

Department of Physics, Amrit Campus, Tribhuvan University, Kathmandu, 44600, Nepal

\*Corresponding author: [dinesh.chaudhary@ac.tu.edu.np](mailto:dinesh.chaudhary@ac.tu.edu.np)

Published online: 25 August 2021

To cite this article: Joshi, L. P. et al. (2021). Green synthesis of zinc oxide nanoparticles using *Ixora Coccinea* leaf extract for ethanol vapour sensing. *J. Phys. Sci.*, 32(2), 15–26. <https://doi.org/10.21315/jps2021.32.2.2>

To link to this article: <https://doi.org/10.21315/jps2021.32.2.2>

**ABSTRACT:** *This article reports the effects of natural plant proteins on the morphology of zinc oxide nanoparticles (ZnONPs) prepared via a precipitation method. Green synthesised ZnONPs have a wide range of uses such as biomedical applications, water purification, optical devices and gas sensors. The non-toxic and economical technique described in this article is favourable for large-scale production too. ZnONPs were produced from a zinc acetate precursor with dye extract of *Ixora Coccinea* (IC) leaves as a capping agent. The as-prepared ZnONPs were characterised by X-ray diffraction (XRD), Fourier transform infrared (FTIR), UV-visible (UV-vis), scanning electron microscopy (SEM) and energy dispersive X-ray (EDX) techniques. The XRD analysis showed an average crystallite size of 23 nm. The SEM analysis revealed a reduction in aggregation of ZnO crystallites due to addition of dye extracts of IC. EDX and UV-vis results confirmed the formation of pure ZnONPs. Finally, the gas sensing properties of ZnO films, prepared by doctor blade method, were used to detect ethanol vapour. The results showed gas response ratios of 28.7 and 5.4 at 800 ppm and 40 ppm exposure, respectively. Furthermore, the response time and recovery time were found to be 24 sec and 47 sec, respectively at 200 ppm exposure of ethanol vapour.*

**Keywords:** green synthesis, metal oxide semiconductor, nanoparticles, *Ixora Coccinea*, gas response

## 1. INTRODUCTION

Nanomaterials are classified based on their size. Their size ranges from one to a few hundred nanometers. Materials at this scale show enhanced physical and chemical properties as compared to their bulk size. Nanoparticles of metal and metal oxide semiconductors (MOS) such as silver, iron oxide, tin oxide and zinc oxide are currently being used in several technologies such as photocatalytic dye degradation, biomedical and optoelectronic devices and gas sensing.<sup>1-5</sup> Among various MOS nanoparticles, zinc oxide nanoparticles (ZnONPs) have garnered significant attention for their use in applications such as gas sensors, biosensors, pollution control and piezoelectric devices. This is primarily because of their high mobility and reactivity, biocompatibility and high chemical and thermal stability.<sup>6-7</sup> As such ZnONPs present an opportunity to further develop material science.

ZnO possesses fascinating properties such as a large band gap (3.37 eV) and exciton binding energy (60 meV), high transparency and easy tuning of electrical and optical behaviour. ZnO can be prepared to different morphologies such as nanoflowers, nanoparticles, nanosheets, nanorods, nanowires and hexagonal prismatic crystals using various conventional and new green synthesis methods.<sup>8-11</sup> Many of the available conventional physical and chemical processes used to synthesis metal oxide semiconductor nanoparticles (MOSNPs) are expensive and energy intensive.<sup>9</sup> They also produce substantial quantities of toxic byproducts, prompting concerns for waste storage and removal. On the other hand, the green synthesis method, wherein plant extracts are used to prepare metal and metal oxide nanoparticles, is a cost-effective and alternative route with a reduced toxic waste load.<sup>12-20</sup> Currently, ZnONPs have been synthesised using the extracts of *Aloe barbadensis miller*, *Black tea*, *Citrus aurantifolia*, *Peltophorumpterocarpum*, *Cyanometraramiflora* and surfactants such as sodium dodecyl sulfate (SDS), cetyltrimethylammonium bromide (CTAB).<sup>21-26</sup> However, there has been limited work done on the synthesis of ZnONPs using dye extracts of the leaves from *Ixora Coccinea* (IC).<sup>27</sup>

Since the sensing performance of ZnO sensor depends on the interactions of gas molecules with the adsorbed oxygen ions ( $O_2^-$  or  $O^-/O^{2-}$ ) on its surface, the surface morphology of ZnO plays an important role. The surface structure of ZnO can be modified by strategies like metal doping and surface treatment.<sup>28-29</sup> Among them, the addition of proteins and other phytochemicals from the natural plant is considered a significant one as it enhances the stability of the nanoparticles.<sup>19</sup> In this process, the extract's presence not only aids in controlling the growth parameters such as aggregation of crystallites but also forms pure and narrow

particle size distributed materials.<sup>27</sup> The present study describes the preparation of ZnONPs using dye extracts of IC leaves, its characterisation and its utilisation in the detection of ethanol vapour.

## **2. EXPERIMENTAL**

### **2.1 Materials**

IC leaves were collected from Calicut, Kerala, India. The most significant compounds in this plant extract are its hydroxyl and carbonyl groups. The phenolics and alkaloids present in the extract are responsible for capping the ZnO nanoparticles.<sup>27</sup> Zinc acetate dehydrate was used as a metal ion precursor and sodium hydroxide (NaOH) as a precipitating agent.

### **2.2 Preparation of the Dye Extract**

First, fresh leaves of the IC plant were washed several times with distilled water. Then, they were dried and grinded at room temperature. Ten grams of grinded leaves were mixed with 40 ml of distilled water and heated to 60°C for 30 min, followed by filtration to remove the solid extract. Finally, the fine solution of dye extract of IC was preserved in a vessel for further study.

### **2.3 Preparation of ZnONPs and Film**

An aqueous solution of 0.5M zinc acetate dehydrate was mixed with 10 ml of above-prepared dye extract. The 2.0M NaOH was added drop wise to this solution while stirring continuously for 2 h. The pH of the mixture solution was maintained at 12. The precipitate was then washed and left for a day for sedimentation to occur. Afterward, it was separated from the upper supernatant liquid by a simple decantation process followed by centrifuging vigorously four times at 1,500 rpm for 10 min each. Finally, the yield was dried at 100°C in a dry air oven for 16 h. A sample of ZnONPs without the dye extract was also prepared following the same procedure for comparison. Both sets, ZnONPs with IC and ZnONPs without IC, were then deposited on a transparent conducting fluorine-doped tin oxide (FTO) substrate using the conventional doctor blade method. The deposited ZnO films were annealed at 550°C inside the muffle furnace. Finally, the film's sensing performances were tested with various concentrations of ethanol vapour.

### 3. RESULTS AND DISCUSSION

#### 3.1 X-ray Diffraction (XRD)

The structural properties of ZnONPs prepared by the precipitation method were studied using XRD with Bruker D2 Phaser (Germany) Diffractometer of Cu- $K_{\alpha}$  radiation of wavelength 1.54184 Å at 30 kV operating voltage and 10 mA current in the  $2\theta$  range of  $20^{\circ}$  to  $80^{\circ}$  at a scanning rate of 0.33 degree per second at Charotar University of Science & Technology, CHARUSAT-Campus, India.

The crystallite size ( $D$ ) was calculated using Debye Scherrer's formula:  $D = \frac{0.9\lambda}{\beta \cos \theta}$

where 0.9 is the correction factor,  $\lambda$  is the wavelength of the X-radiation,  $\beta$  is the full width half maximum (FWHM) measured in radian of the diffraction peak and  $\theta$  is the Bragg's angle.<sup>14</sup> The XRD powder patterns of ZnONPs prepared with and without IC are shown in Figure 1. The figure illustrated multiple peaks oriented along (100), (002), (101), (102), (110), (103), (200), (112), (201), (004) and (202). All the peaks are indexed concerning the standard JCPDS values of card number 36-1451.<sup>24</sup> The multiple sharp peaks observed in the XRD patterns are characteristics of the polycrystalline nature of ZnO. The calculated values of average crystallite size ( $D$ ) and lattice parameters of both sets of ZnONPs are shown in Table 1. The result showed the average value of  $D$  was 23.80 nm for ZnONPs prepared with IC and 22.02 nm for ZnONPs without IC. The  $c/a$  ratio

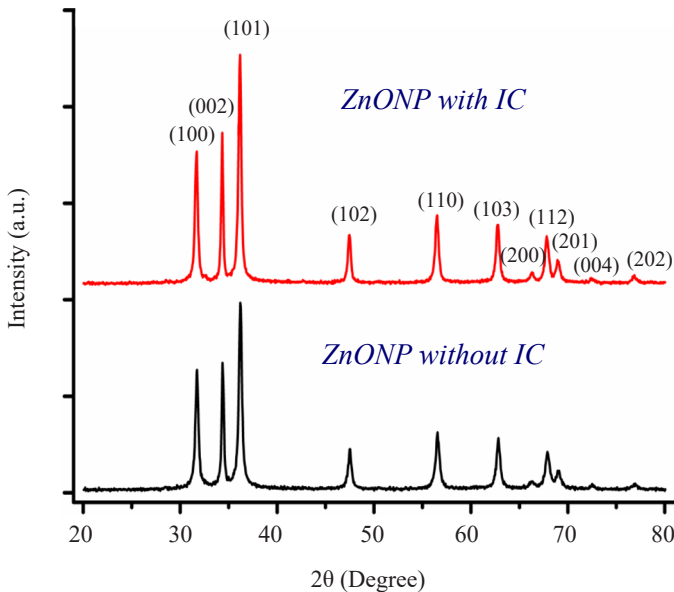


Figure 1: XRD patterns of as-prepared ZnONPs.

for both samples was 1.6 suggesting the wurtzite hexagonal phase of ZnO. There was no observation of other impurity peaks in the XRD pattern, proving that the as-prepared ZnONPs are of high purity.

Table 1: Calculated average crystallite size and lattice parameters of ZnONPs.

Samples	Average crystallite size (nm)	Lattice parameters (Å)	
		a	c
ZnONP with IC	23.08	3.01547	5.2229
ZnONP without IC	22.02	3.25662	5.2150

### 3.2 Scanning Electron Microscopy (SEM)

Figure 2(a) and 2(b) illustrates the SEM images of ZnONPs prepared without and with dye extract at a resolution of 200 nm. The captured images revealed the aggregated clusters of ZnO crystallites.<sup>24</sup> Figure 2(b) clearly shows the less aggregated morphology of ZnONPs which was due to the presence of IC extract acting as a capping agent.

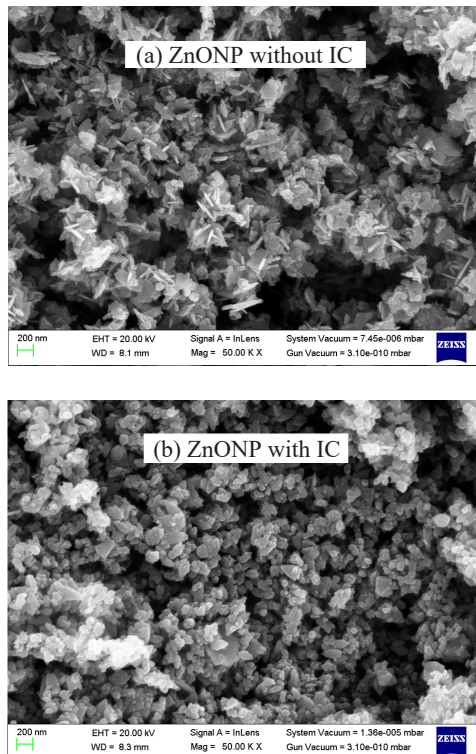


Figure 2: SEM images ZnONPs (a) without IC and (b) with IC.

### 3.3 Energy Dispersive X-ray (EDX) Analysis

The results of the EDX performed to uncover the elemental composition of the synthesised ZnONPs with and without dye extract, are portrayed in Figure 3. The figure clearly shows two sharp peaks at 1.0 keV and 8.5 keV and a lower one at 0.5 keV, the characteristic features of zinc and oxygen. These results agreed with the reported values.<sup>13</sup> The atomic percentage of the present elements were 55.43% of zinc and 44.57% of oxygen in bare ZnONPs (Figure 3[a]) and 53.80% of zinc and 46.20% of oxygen for ZnONPs prepared with IC (Figure 3[b]). The results confirmed the high purity of as-synthesised ZnONPs.

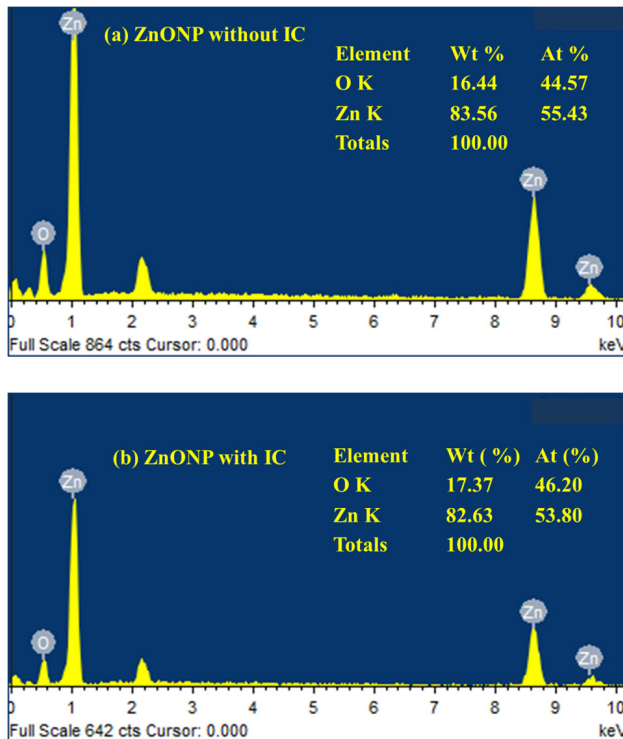


Figure 3: EDX spectra of ZnONPs (a) without IC and (b) with IC.

### 3.4 Fourier Transforms Infrared (FTIR) and UV-Visible (UV-vis) Spectroscopy

Figure 4(a) depicts the FTIR spectrum of ZnONPs synthesised with IC in the wavenumber range of  $400\text{ cm}^{-1}$  to  $4,000\text{ cm}^{-1}$ . It clearly shows major bands at  $400\text{ cm}^{-1}$ ,  $574\text{ cm}^{-1}$ ,  $880\text{ cm}^{-1}$ ,  $1,407\text{ cm}^{-1}$ ,  $1,628\text{ cm}^{-1}$  and  $3,420\text{ cm}^{-1}$ . The sharp infrared (IR) band extends from  $400\text{ cm}^{-1}$

to  $650\text{ cm}^{-1}$  corresponding to metal oxide vibration confirmed the formation of ZnONPs. The peak at  $880\text{ cm}^{-1}$  indicated the alkane  $\text{sp}^2$  hybridised  $=\text{C-H}$  bond and the alkane  $\text{sp}^3$  hybridised  $\text{C-H}$  bond bending, respectively.<sup>12</sup> The peaks in the regions  $1,407\text{ cm}^{-1}$  and  $1,628\text{ cm}^{-1}$  were ascribed to the vibrating, stretching, and bending modes of water molecules present in the sample respectively. Finally, a huge depression peak at  $3,420\text{ cm}^{-1}$  showed the presence of hydroxyl group.<sup>13</sup> The UV-vis absorption spectrum was captured using an Ocean Optics spectrophotometer (Model: HR4000CG-UV-NIR, Singapore), to confirm the formation of ZnONPs as depicted in Figure 4(b). The peak observed at  $340\text{ nm}$  ascertained the formation of ZnONPs.

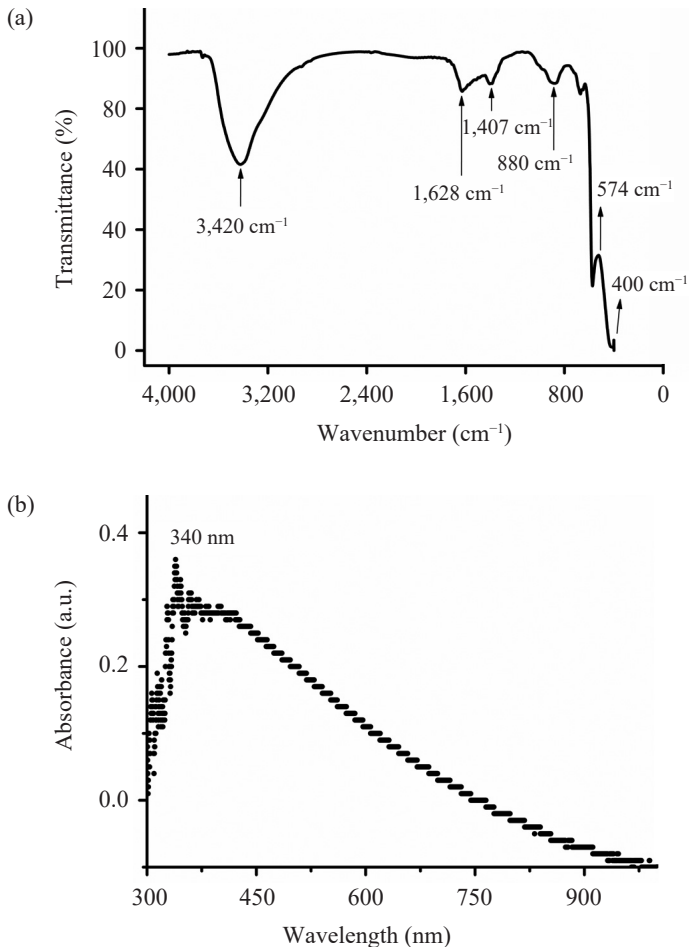


Figure 4: (a) FTIR and (b) absorbance of ZnONPs prepared with dye extract of IC.

### 3.5 Sensitivity Measurements

The gas response was calculated by measuring the ratio of  $R_a/R_g$ , where  $R_a$  and  $R_g$  are the resistances of ZnO measured in air and gas, respectively. The electrical resistance of MOS is a temperature-sensitive property so its working temperature must be optimised.<sup>29</sup> Figure 5(a) shows the optimised temperature of 285°C for both samples. Figure 5(b) illustrated the linear increment of gas response with increasing gas concentration measured at its optimised temperature. The measured values of gas response, response and recovery times were shown in Table 2. It shows a gas response of 28.7 for ZnO with IC and 37.4 for ZnO without IC at 800 ppm of ethanol exposure. The difference in these values may be due to the change in the morphology of ZnO. The gas response ratios were 5.4 and 3.5 for 40 ppm exposure of ethanol vapour. The inset in Figure 5(b) shows the response and recovery times of ZnO sensors with 200 ppm exposure of ethanol vapour for clarity. The response and recovery times were respectively 24 sec and 47 sec for ZnO with IC, whereas these values were respectively 21 sec and 27 sec for ZnO without IC.

Table 2: Gas response, response and recovery times of the ZnO sensors.

Concentration of ethanol (ppm)	ZnO without IC			ZnO with IC		
	Response $R_a/R_g$	Response time (sec)	Recovery time (sec)	Response $R_a/R_g$	Response time (sec)	Recovery time (sec)
40	3.50	15	33	5.47	23	50
80	3.97	21	27	5.56	26	51
120	4.38	23	23	6.22	25	49
160	6.20	23	25	9.94	27	46
200	19.28	21	27	10.23	24	47
400	26.16	24	27	13.63	27	49
800	37.43	19	25	28.76	26	49

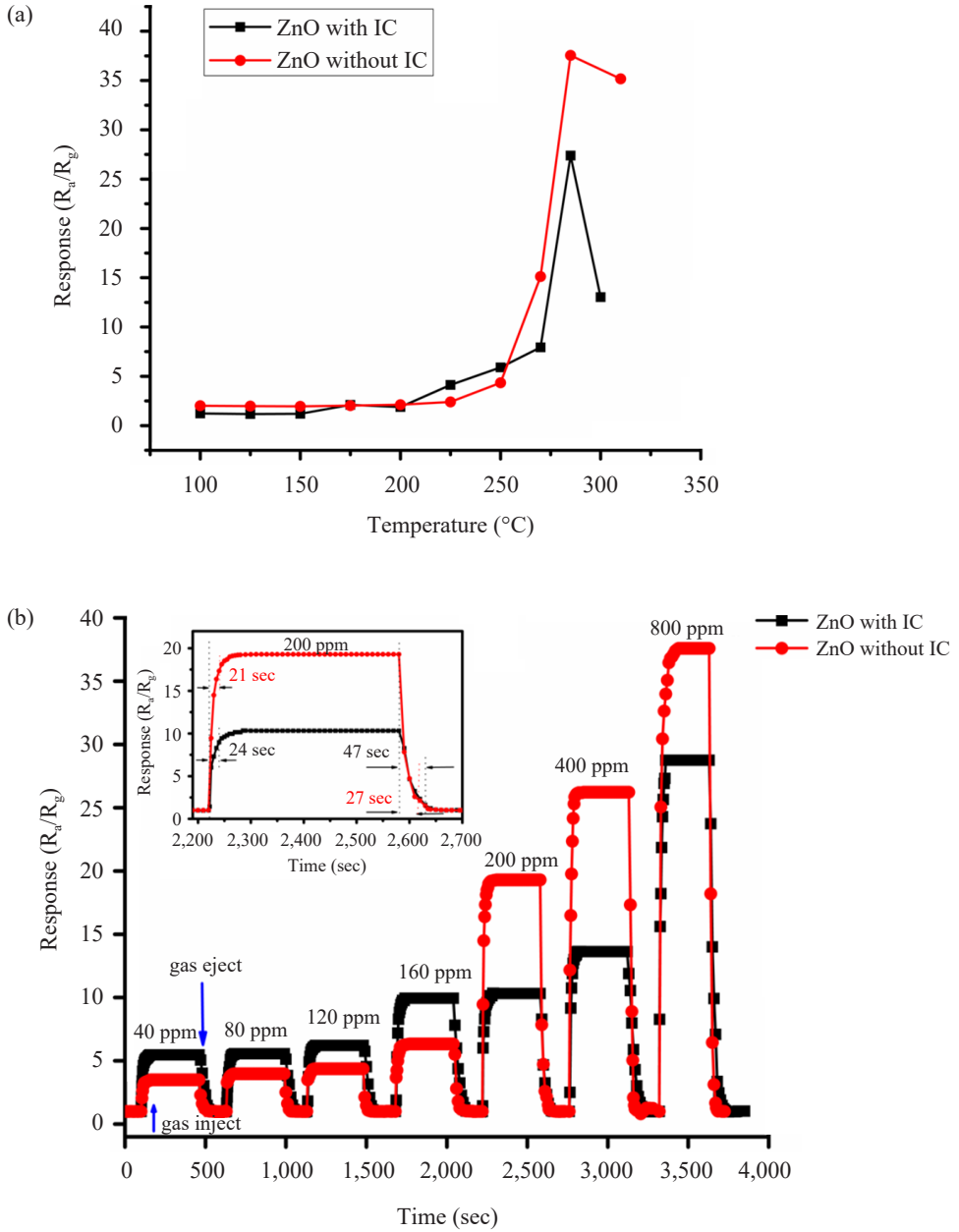


Figure 5: Response characteristics of ZnO film as a function of (a) temperature and (b) gas concentration.

#### 4. CONCLUSION

ZnONPs were successfully fabricated using dye extract of IC leaves as a capping agent by precipitation method. Investigations of morphology, structure and dimension of ZnONPs were performed by SEM, XRD and UV-vis analyses. The average crystallite size of ZnONPs was found to be 23 nm. The SEM investigation illustrated the change in morphology of ZnO from highly clustered to less aggregate clustered of ZnO crystallites after IC dye extract was added. Furthermore, the presence of hydroxyl groups, ZnO bands and the percentage content of zinc and oxygen were established by FTIR and EDX, respectively. The sensitivity results of ZnO film prepared with IC showed a gas response ratio of 28.7 and 5.4 for the exposure of 800 ppm and 40 ppm of ethanol vapour, respectively.

#### 5. ACKNOWLEDGEMENTS

The authors would like to thank the University Grants Commission (UGC), Nepal for providing financial support under FRG-73-74-S & T-09 to complete this research work. The authors would also like to thank Charotar University of Science and Technology CHARUSAT-Campus and the Indian Institute of Technology (IIT), India for the support in conducting FTIR, XRD, SEM and EDX experiments.

#### 6. REFERENCES

1. Vinayagam, R. et al. (2020). Structural characterization of green synthesized  $\alpha$ -Fe<sub>2</sub>O<sub>3</sub> nanoparticles using the leaf extracts of *Spodias dulcis*. *Surf. Interface*, 20, 100618. <https://doi.org/10.1016/j.surfin.2020.100618>
2. Varadavenkatesan, T., Selvaraj, R. & Vinayagam, R. (2020). Green synthesis of silver nanoparticles using *Thunbergia gradiflora* flower extract and its catalytic action in reduction of Congo red dye. *Mater. Today: Proceeds.*, 23(1), 39–42. <https://doi.org/10.1016/j.matpr.2019.05.441>
3. Bhatia, S., Verma, N. & Bedi, R. K. (2017). Ethanol gas sensor based upon ZnO nanoparticles prepared by different techniques. *Results in Phys.*, 7, 801–806. <https://doi.org/10.1016/j.rinp.2017.02.008>
4. Inderan, V. et al. (2019). A comparative study of structural and ethanol gas sensing properties of pure, nickel and palladium doped SnO<sub>2</sub> nanorods synthesized by the hydrothermal method. *J. Phys. Sci.*, 30(1), 127–143. <https://doi.org/10.21315/jps2019.30.1.10>
5. Hamady, S. O. S. et al. (2019). Development of novel thin film solar cells: Design and numerical optimization. *J. Phys. Sci.*, 30 (Supp.2), 199–205. <https://doi.org/10.21315/jps2019.30.s2.17>

6. Fardood, S. T. et al. (2020). Facile green synthesis and characterization of zinc oxide nanoparticles using tragacanthgel: Investigation of their photocatalytic performance for dye degradation under visible light irradiation. *Nanochem. Res.*, 5(1), 69–76. <https://doi.org/10.22036/ncr.2020.01.007>
7. Wang, X. et al. (2006). Piezoelectric field effect transistor and nanoforce sensor based on a single ZnO nanowire. *Nano Lett.* 6(12), 2768-2772. <https://doi.org/10.1021/nl061802g>
8. Vinayagam, R. et al. (2020). Synthesis, characterization and photocatalytic dye degradation capability of *Calliandra haematocephala* mediated zinc oxide nanoflowers. *J. Photochem. and Photobiol. B: Biol.*, 203, 111760. <https://doi.org/10.1016/j.jphotobiol.2019.111760>
9. Liu, X. et al. (2004). Growth mechanism and properties of ZnO nanorods synthesized by plasma-enhanced chemical vapor deposition. *J. Appl. Phys.*, 95(6), 3141–3147. <https://doi.org/10.1063/1.1646440>
10. Fardood, S. T. et al. (2019). Green synthesis of ZnO nanoparticles via sol-gel method and investigation of its application in solvent-free synthesis of 12-Aryltetrahydrobenzo[*a*] xanthene-11-one derivatives under microwave irradiation. *Chem. Method.*, 3, 632–642. <https://doi.org/10.33945/SAMI/CHEMM.2019.6.2>
11. Li, S.-M. et al. (2017). Acetone sensing of ZnO nanosheets synthesized using room-temperature precipitation. *Sens. Actuators B: Chemical*, 249, 611–623. <http://doi.org/10.1016/j.snb.2017.04.007>
12. Vinayagam, R., Varadavenkatesan, T. & Selvaraj, R. (2017.) Green synthesis, structural characterization and catalytic activity of silver nanoparticles stabilized with *Bridelia retusa* leaf extract. *Green Process Synth.*, 7(1), 1–8. <https://doi.org/10.1515/gps-2016-0236>
13. Sirdeshpande, K. D. et al. (2018). Structural characterization of mesoporous magnetite nanoparticles synthesized using the leaf extract of *Calliandra haematocephala* and their photocatalytic degradation of malachite green dye. *Appl. Nanosci.*, 8(4), 675–683. <https://doi.org/10.1007/s13204-018-0698-8>
14. Fardood, S. T. et al. (2020). Green synthesis, characterization, and photocatalytic activity of cobalt chromite spinel nanoparticles. *Mater. Res. Express.*, 7, 015086. <https://doi.org/10.1088/2053.1591/ab6c8d>
15. Gawade, V. V. et al. (2017). Green synthesis of ZnO nanoparticles by using *Calotropis procera* leaves for the photo-degradation of methyl orange. *J. Mater. Sci. Mater. Electron*, 28, 14033–14039.
16. Fardood, S. T. et al. (2019). Biosynthesis of MgFe<sub>2</sub>O<sub>4</sub> magnetic nanoparticles and their application in photodegradation of malachite green dye and kinetic study. *Nanochem. Res.*, 4(1), 86–93. <https://doi.org/10.22036/ncr.2019.01.010>
17. Fardood, S. T. et al. (2019). Eco-friendly synthesis and characterization of  $\alpha$ -Fe<sub>2</sub>O<sub>3</sub> nanoparticles and study of their photocatalytic activity for degradation of Congo red dye. *Nanochem. Res.*, 4(2), 140–147. <https://doi.org/10.22036/ncr.2019.02.005>

18. Atrak, K., Ramazani, A. & Fardood, S. T. (2019). Green synthesis of  $Zn_{0.5}Ni_{0.5}AlFeO_4$  magnetic nanoparticles and investigation of their photocatalytic activity for degradation of reactive blue 21 dye. *Environ. Technol.*, 41(21), 1581841. <https://doi.org/10.1080/09593330.2019.1581841>
19. Azar, B. E., Fardood S. T. & Morsali, A. (2019). Green synthesis and characterization of  $ZnAl_2O_4@ZnO$  nanocomposite and its environmental applications in rapid dye degradation. *Optik*, 208, 164129. <https://doi.org/10.1016/j.ijleo.2019.164129>
20. Vanathi, P. et al. (2014). Biosynthesis and characterization of phyto mediated zinc oxide nanoparticles: A green chemistry approach. *Mater. Lett.*, 134, 13–15. <https://doi.org/10.1016/j.matlet.2014.07.029>
21. Sangeetha, G., Rajeshwari, S. & Venckatesh, R. (2011). Green synthesis of zinc oxide nanoparticles by aloe barbadensis miller leaf extract: Structure and optical properties. *Mater. Res. Bull.*, 46, 2560–2566. <https://doi.org/10.1016/j.materresbull.2011.07.046>
22. Fardood, S. T., Ramazani, A. & Joo, S. W. (2017). Sol-gel synthesis and characterization of zinc oxide nanoparticles using Black Tea extract. *J. Appl. Chem. Res.*, 11(4), 8–17. [http://jacr.kiau.ac.ir/article\\_536676.html](http://jacr.kiau.ac.ir/article_536676.html)
23. Samat, N. A. & Nor, R. M. (2013). Sol–gel synthesis of zinc oxide nanoparticles using Citrus aurantifolia extracts. *Ceram. Int.*, 39, S545–S548. <https://doi.org/10.1016/j.ceramint.2012.10.132>
24. Pai, S. et al. (2019). Photocatalytic zinc oxide nanoparticles synthesis using Peltophorum pterocarpum leaf extract and their characterization. *Optik*, 185, 248–255. <https://doi.org/10.1016/j.ijleo.2019.03.101>
25. Ramimoghadam, D., Hussein, M. Z. B. & Taufiq-Yap, Y. H. (2012). The effect of sodium dodecyl sulfate (SDS) and cetyltrimethylammonium bromide (CTAB) on the properties of ZnO synthesized by hydrothermal method. *Inter. J. Mol. Sci.*, 13, 13275–13293. <https://doi.org/10.3390/ijms131013275>
26. Varadavenkatesan, T. et al. (2019). Photocatalytic degradation of Rhodamine B by zinc oxide nanoparticles synthesized using the leaf extract of *Cyanometra ramiflora*. *J. Photochem. & Photobiol. B: Biol.*, 199, 111621. <https://doi.org/10.1016/j.jphotobiol.2019.111621>
27. Yedurkar, S., Maura, C. & Mahanwar, P. (2016). Biosynthesis of zinc oxide nanoparticles using *Ixora Coccinea* leaf extract—a green approach. *Open J. Synth. Theo. Appl.*, 5(1), 1–14. <https://doi.org/10.4236/ojsta.2016.51001>
28. Paraguay, F. et al. (2000). Influence of Al, In, Cu, Fe and Sn dopants on the response of thin film ZnO gas sensor to ethanol vapor. *Thin Solid Films*, 373, 137–140. [https://doi.org/10.1016/S0040-6090\(00\)01120-2](https://doi.org/10.1016/S0040-6090(00)01120-2)
29. Wei, A., Pan, V. & Huang, W. (2011). Recent progress in the ZnO nanostructure-based sensors. *Mater. Sci. Eng. B*, 176(18), 1409–1421. <https://doi.org/10.1016/j.mseb.2011.09.005>